

Velocity Gradients in the Intracluster Gas of the Perseus Cluster

Renato A. Dupke & Joel N. Bregman
University of Michigan, Ann Arbor, MI 48109-1090

ABSTRACT

We report the results of spatially resolved X-ray spectroscopy of 8 different ASCA pointings distributed symmetrically around the center of the Perseus cluster. The outer region of the intracluster gas is roughly isothermal, with temperature $\sim 6\text{--}7$ keV, and metal abundance ~ 0.3 Solar. Spectral analysis of the central pointing is consistent with the presence of a cooling flow and a central metal abundance gradient. A significant velocity gradient is found along an axis at a position angle of $\sim 135^\circ$, which is $\sim 45^\circ$ discrepant with the major axis of the X-ray elongation. The radial velocity difference is found to be greater than $1000 \text{ km s}^{-1} Mpc^{-1}$ at the 90% confidence level. Simultaneous fittings of GIS 2 & 3 indicate that the velocity gradient is significant at the 95% confidence level and the F-test rules out constant velocities at the 99% level. Intrinsic short and long term variations of gain are unlikely ($P < 0.03$) to explain the velocity discrepancies.

Subject headings: galaxies: clusters: individual (Abell 426) — intergalactic medium — cooling flows — X-rays: galaxies —

1. Introduction

X-ray determination of the physical state of the intracluster gas provides a unique tool to probe the origin and evolution of clusters of galaxies. ASCA observations have shown significant spatial temperature variations in many clusters, indicating that clusters are currently evolving systems. This is consistent with the predictions of hierarchical cluster formation within CDM models, and had been suggested in pre-ASCA times (e.g. Fitchett 1988, Ulmer, Wirth & Kowalski 1992 and references therein).

Although early models of galaxy clusters treated them as spherically symmetric virialized systems, recent X-ray and optical studies show that often clusters show substructures. Furthermore, if cold dark matter models (CDM) are correct, primordial small-scale density fluctuations are not erased and clusters are formed by infall/merging of smaller scale objects (bottom-up hierarchical scenario). The merger (infall) of sub-clumps creates shocks (associated with temperature substructure), bulk gas flows (associated with velocity substructure) and asymmetric distributions of velocity of galaxies (e.g. Bird 1993). In order to understand the physical properties of clusters, their origin and evolution one has to take into account the degree and the physical scale of substructuring. Furthermore, the degree of substructuring itself can be used to determine/constrain cosmological parameters (Crone, Evrard & Richstone 1996).

Measurements of substructure using spatially resolved X-ray spectra have some advantages over optical analysis of galaxies in clusters. Firstly, one does not need a large number of galaxies' redshifts in a cluster. Secondly, the velocity mapping of the ICM is not biased by the inclusion of foreground/background galaxies (outliers), which may bias the statistical analysis for measuring substructures (e.g. Fitchett 1988, Bird 1993). The determination of complex temperature substructure in clusters is often interpreted to be related to shocks due to cluster merger at different stages. The link between temperature substructure and the merger stage is often done by comparison with hydrodynamical simulations. There are currently an enormous variety (different initial conditions, hydro-codes, impact parameters, matter components, etc.) of cluster formation/merger simulations in the literature (e.g. Evrard 1990; Katz & White 1993; Roettiger, Burns & Loken 1993, 1996; Schindler & Muller 1993; Pearce, Thomas & Couchman 1994; Navarro, Frenk & White 1995; Evrard, Metzler, & Navarro 1996; Roettiger, Loken & Burns 1997, Ricker 1998; Takizawa & Mineshige 1998; Takizawa 1999, 2000 and references therein), which can be used to compare with the observations.

A more straightforward way to determine the effects of a merger is to directly measure intracluster gas bulk velocities. Several simulations of cluster mergers indicate residual gas velocities of a few thousand km s^{-1} (e.g. Ricker 1998, Roettiger et al. 1993, Takizawa 1999,

Roettiger & Flores 2000). To measure gas velocities one requires accurate determinations of spectral line centroids. The precision with which a line centroid can be measured, in velocity space, is $\sim 127 \Gamma_{eV} (E_{keV} N^{\frac{1}{2}})^{-1}$ km s $^{-1}$, where N is the number of photons in the line and Γ_{eV} is the FWHM of the line, or if the line is narrower than the instrumental width, is the FWHM of the instrument, and E_{keV} is the line energy. The energy resolution of the spectrometers on-board *ASCA* vary from 2% (SIS) to 8% (GIS) at 5.9 keV. For a FWHM of 9000 km s $^{-1}$ at 6.7 keV, which is typical of early (first 3 years) SIS data at the FeK α line), to obtain a line centroid to a precision of 500 km s $^{-1}$ we need ~ 60 line photons. This same accuracy can be obtained with the GIS with ~ 350 line photons¹. Although several clusters observed by *ASCA* match this requirement, when observing regions within the detector field of view, the flux in the outer regions of the detector is dominated by photons coming from central regions due to the extended *ASCA* PSF and if there are strong radial velocity gradients the latter effect would make redshift determinations unprecise. Therefore, ideally, one would like to analyze high-metal abundance clusters that have several different long-exposure observations from off-center regions surrounding the cluster's X-ray center. Some nearby clusters match this criteria and, therefore, are well suited for the study of gas velocity distribution. Perseus is an ideal target for this analysis since it is a nearby very bright cluster. Furthermore, it has been observed extensively by *ASCA* with a large number of offset pointings, covering a more or less symmetrical region around the cluster's center up to distances of $> 1 h_{50}^{-1}$ Mpc.

In this work we analyze the spectra of 8 separate pointings encompassing a region of $> 40'$ radius around the center of the Perseus cluster. We find that although the cluster is roughly isothermal (aside from the cooling flow) there is a significant velocity gradient along a direction that has an inclination $\geq 50^\circ$ with respect to the cluster's X-ray major axis. This velocity gradient is consistent with a rotation velocity of ≥ 1000 km s $^{-1}$ at the 90% confidence level and is unlikely to be caused by gain variations or background sources.

2. The Perseus Cluster

The Perseus cluster has been the subject of many studies since its discovery as an X-ray source by Fritz et al. (1971). It is one of the closest (at an optical redshift of 0.0183), X-ray bright, rich cluster of galaxies. The cluster is elongated and the ratio of its minor to major axis is 0.83 at radii greater than 20' (Snyder et al. 1990). It has a cooling flow with a mass deposition rate of about $(3-5) \times 10^2 M_\odot \text{ yr}^{-1}$ (Allen et al. 1992; Peres et al. 1998;

¹These estimates become more uncertain if the rms of the continuum starts to compete with the line.

Ettori, Fabian & White 1998). The centroid of the cluster emission is offset by $\sim 2'$ to the east of NGC 1275 (Snyder et al. 1990, Branduardi-Raymond et al. 1981). The average temperature of the X-ray emitting gas is approximately 6.5 keV (Eyles et al. 1991) and the average abundance is 0.27 Solar in the central 1 degree (Arnaud et al. 1994).

The existence of an iron abundance gradient in Perseus was first suggested by Ulmer et al. (1987) using data from SPARTAN 1. They found an iron abundance of ~ 0.81 Solar and a temperature of ~ 4.16 keV within the central $5'$ and an abundance of ~ 0.41 solar and a temperature of ~ 7.1 keV in the outer regions ($6 - 20'$). Further analyses have corroborated the existence of an abundance gradient (e.g. Ponman et al. (1990), Kowalski et al. (1993), Arnaud et al. 1994, Dupke & Arnaud 2000). Furthermore, the region where the abundance is enhanced is predominantly enriched by SN Ia ejecta (Dupke & Arnaud 2000), indicating that the cluster belongs to the class of clusters that present central “chemical gradients”, such as A496 (Dupke & White 2000). The presence of cooling flows, global abundance and chemical gradients suggest that the cluster has not undergone strong mergers recently.

3. Data Reduction & Analysis

ASCA carries four large-area X-ray telescopes, each with its own detector: two Gas Imaging Spectrometers (GIS) and two Solid-State Imaging Spectrometers (SIS). Each GIS has a $50'$ diameter circular field of view and a usable energy range of 0.8–10 keV; each SIS has a $22'$ square field of view and a usable energy range of 0.5–10 keV. The nominal energy resolution of the spectrometers are 8% and 2% at 5.9 keV for GISs and SISs, respectively. The SISs energy resolution is steadily degrading with time (e.g. Dottani et al. 1997) and for most pointings analyzed in this work is $\geq 4\%$ at 5.9 keV. Eight individual pointings were analyzed in this work. The central pointing is the only one that includes the contaminating source (the center of the Perseus cluster). The other seven pointings are distributed more or less symmetrically around the central pointing with an average distance of $\sim 40'$ from the center. Five of the pointings (the most recent ones) were consecutively observed in 1997 and are spaced in time typically by a day. The pointing characteristics are listed in Table 1 and shown in Figure 1.

We selected data taken with high and medium bit rates, with cosmic ray rigidity values ≥ 6 GeV/c, with elevation angles from the bright Earth of $\geq 20^\circ$, and from the Earth’s limb of $\geq 5^\circ$ (GIS); we also excluded times when the satellite was affected by the South Atlantic Anomaly. Rise time rejection of particle events was performed on GIS data. The resulting effective exposure times are also shown in Table 1. We estimated the background from blank sky files provided by the ASCA Guest Observer Facility and removed bright

point sources for each instrument in all pointings.

The SISs have a better spectral resolution (by a factor of 2–4) than the GISs. However, the analysis of SIS data for our pointings is severely limited by photon statistics (the GISs overall count rate is typically more than ten times that of the SISs), making the SIS redshift determination very uncertain. This difference in count rate between GISs and SISs is due to the following reasons: 1) most of the pointings analyzed in this work were observed by the SIS in 2-CCD mode, which minimizes the energy resolution degradation due to the residual dark-current distribution and non-uniform charge transfer inefficiency effects²; 2) there have been increasing discrepancies between SIS and GIS spectra below 1 keV since 1994, due to a decrease in X-ray efficiency in the SISs, thus making the low end (<0.9 keV) of the spectral region unusable for the SISs³; 3) the X-ray center of Perseus is not in the detector’s field of view for all outer pointings analyzed and, therefore, most of the photons come from a specific direction (towards the cluster’s center). Furthermore, the GISs have a higher effective area at high energies. Therefore, we use only GIS 2 & 3 in this analysis.

In the spectral fittings we used **XSPEC** v10.0 (Arnaud 1996) software to analyze the GIS spectra separately and jointly (simultaneous fittings of data from GIS 2&3). The spectra were fitted using the **mekal** thermal emission models, which are based on the emissivity calculations of Mewe & Kaastra (cf. Mewe, Gronenschild & van den Oord 1985; Mewe, Lemen & van den Oord 1986; Kaastra 1992), with Fe L calculations by Liedahl, Osterheld & Goldstein (1995). Abundances are measured relative to the solar photospheric values of Anders & Grevesse (1989), in which $\text{Fe}/\text{H}=4.68 \times 10^{-5}$ by number. Galactic photoelectric absorption was incorporated using the **wabs** model (Morrison & McCammon 1983); Spectral channels were grouped to have at least 25 counts/channel. Energy ranges were restricted to 0.8–9 keV for the GISs.

Since there is a cooling flow at the center of Perseus we added a cooling flow component (Mushotzky & Szymkowiak 1988) to the **mekal** thermal emission model in the central pointing, to compare the temperature of the hot component in the center with that of the outer pointings. We adopted the emission measure temperature distribution that corresponds to isobaric cooling flows. We tied the maximum temperature of the cooling flow to the temperature of the thermal component, and we fixed the minimum temperature at 0.1 keV. The abundances of the two spectral components (**mekal** and **cflow**) were tied together. We also applied a single (but variable) global absorption to both spectral components. Since the cD galaxy of Abell 426 (NGC 1275) is an AGN, we also included a

²heasarc.gsfc.nasa.gov/docs/asca/newsletters/sis_calibration5.html

³heasarc.gsfc.nasa.gov/docs/asca/watchout.html, also Hwang et al. 1999

power law component in the spectral fittings of the central pointing.

We extracted spectra from a circular region with a radius of $20'$ for each pointing, centered at the detector's center. The best-fit values for temperature, abundance and redshift obtained from spectral fittings of GIS2 and GIS3 separately are consistent with those obtained through the spectral fittings of both GIS 2 & 3 jointly. Therefore, we show here only the best-fit parameters of the simultaneous fittings. The resulting joint fits were very good with reduced $\chi^2_\nu \sim 1$ for all regions.

4. Results

4.1. Spectral Fittings

The best-fit values for temperature, abundance and redshift are shown in Table 2, and plotted in Figure 2 as a function of the azimuthal angle. Here, we define the azimuthal angle with respect to the line that joins the centers of pointings P1(NW) and P5(SE), for convenience. For P1(NW) the azimuthal angle is set to zero. The indicated errors in Figure 2 are 1σ confidence limits. It can be seen that Perseus appears to be roughly isothermal in the outer regions with an average temperature of ~ 7 keV. The dashed and solid lines for the temperature plot in Figure 2 indicate the 1σ confidence levels for the simultaneous GIS 2 & 3 spectral fittings of the central pointing with and without the absorbed cooling flow component, respectively. The central best-fitting temperature for models that include a cooling flow component is not well constrained by the GISs and shows a best-fit value of 6.85 ± 1 keV, which is consistent with the observed temperatures in the outer regions. Since the GISs are not very sensitive to the absorbing column density the absolute values of the best-fitting temperatures may be artificially increased if the best-fit N_H values are low. To test this effect we fixed N_H at its putative Galactic value at the direction of each pointing ($N_H \sim 1.6 \times 10^{21} \text{ cm}^{-2}$, Dickey & Lockman 1990; HEASARC NH Software). The best-fitting temperatures obtained this way have significantly worse χ^2_ν and are also plotted in Figure 2 (open circles). The best-fit temperatures obtained when N_H is free to vary are lower than those obtained with free N_H by ~ 1.5 keV. Although the azimuthal distribution of temperatures is consistent with isothermality, some pointings show mild, but significant, azimuthal variations (e.g. Pointing 7(W), for which the temperature is significantly ($>90\%$ confidence) higher than P6 (S-SW) and P3 (NE) by about a keV).

The abundances observed in the outer parts of Perseus are generally lower than in the central region, which is consistent with observations by other authors (Ulmer et al. 1987; Ponman et al. 1990; Kowalski et al. 1993; Arnaud et al. 1994; Dupke & Arnaud 2000).

The abundance measured in the central pointing is 0.43 ± 0.02 Solar and in the outer parts has an average value of ~ 0.33 Solar. There is marginal evidence of azimuthal abundance variations. In particular, P6 (S-SW) best-fit abundance is higher than the that measured for P2 (N), and is also consistent with the abundance measured in the central region. The best-fit abundances for each pointing are also displayed in Figure 2, where the solid lines represent the 1σ confidence limits for the abundance in the central pointing. The dash-dotted lines show the 90% limits for the abundance measured within a $4'$ region of the center of Perseus for comparison (Dupke & Arnaud 2000).

The most important azimuthal distribution is that of redshifts. Two pointings show significant ($\geq 90\%$ confidence level) discrepant redshifts with respect to the best-fit redshift observed in the central pointing. These two redshift-discrepant pointings, P1(NW) and P5(SE), are on opposite sides of the cluster's center. P1(NW) shows a best-fit redshift of 0.0145 (0.003-0.0185) and P5(SE) shows a significantly higher (95% confidence level) redshift value of 0.042 (0.025-0.045). This redshift discrepancy is observed in both GIS 2 and GIS 3 individually, although with lower statistical significance. These differences in redshifts imply a velocity difference of 8200 (2000 - 12700) km s^{-1} between these two pointings. The azimuthal distribution of redshifts is shown in Figure 2 and the best-fit values are listed in Table 2. In the fittings where the column density is fixed at the Galactic value, the best-fit redshifts are typically lower than those obtained with N_H free. However, the inferred differences between redshifts for different pointings are virtually unaltered. Therefore, the redshift discrepancies are not due to uncertainties related to the GIS sensitivity to hydrogen column densities.

The two redshift-discrepant pointings show no differences in the best-fit values of temperatures or abundances. To further test the significance of the velocity difference between P1 and P5, we simultaneously fit all four spectra (GIS 2 & 3 for each of the two pointings) and applied the F-test in the analysis of χ^2 variations due to the change in the number of degrees of freedom. We compare the χ^2 of fits which assumed the redshifts were the same in the two projected spatial regions $z_{G2_{P1}} = z_{G3_{P1}} = z_{G2_{P5}} = z_{G3_{P5}}$ to that of fits which allowed the redshifts in the two pointings to vary independently. Within the same pointing the redshifts were still locked together for different instruments, i.e., $(z_{G2_{P1}} = z_{G3_{P1}}) \neq (z_{G2_{P5}} = z_{G3_{P5}})$, where $z_{G_i_{P_j}}$ is the redshift of pointing j with instrument GIS i . The difference between the χ^2 of these two fits must follow a χ^2 distribution with one degree of freedom (Bevington 1969). The difference in χ^2 from the fits with locked and unlocked redshifts indicates that the redshifts are discrepant at the 99% level. We show in Figure 3 the 68%, 90% and 99% confidence contours for two interesting parameters (redshifts) of regions P1 and P5 as well as the line correspondent to equal redshifts. The spectral fits within the energy range encompassing the FeK line complex are shown in

Figures 4a,b. We also show in Figures 4a,b the residuals from the same model fittings but with zero metal abundances for illustration.

The inclusion of the power law component in the spectral fittings (representing any non-thermal emission from NGC 1275) in addition to the cooling flow component in the central region (P0) does not change significantly the best-fit values of the redshifts obtained without the power law component. However, it does make the best-fit redshift values less precise. Since the F-test shows that there is a significant improvement in the spectral fittings when the power-law component is included we, conservatively, quote in Table 2 and Figure 2 the values of the best-fit redshift for spectral fittings that included an extra power law component.

4.2. GIS Gain Variations

We have shown in the previous section that the azimuthal distribution of velocities in the Perseus cluster shows significantly ($\geq 90\%$ confidence) different redshifts for three Pointings: the central pointing (P0) and two other diametrically opposed pointings (P1 & P5). However, since the determination of redshifts relies on accurate measurement of line centroids (mainly the FeK line around 6.7 keV), large variations of gain (conversion between photon energy and pulse height) can, in principle, mimic the observed effect. In this section, we estimate the effects of gain variations in our observations.

The original gain calibration of the GISs was mainly based on the built-in Fe-55 isotope source, attached to the edge of the field of view. The gain depends on the temperature of the phototube ($\sim 1\%/\text{ }^{\circ}\text{C}$), the position on the detector and time of observation. During the first several months in orbit the gain decreased by a few percent, and this trend has slowly disappeared. This gain decrease is possibly due of cosmic-ray induced crystalline defects, decreasing the UV transmission of the quartz windows of the gas cell (Tashiro et al. 1995).

The intrinsic GIS gain is not only dependent on temperature but also on position (on the detector) due to non-uniformity in the phototube gain. Therefore, the gain correction process involves a look-up table called the ‘gain map’ (Tashiro et al. 1995 and references therein), which is also dependent on time and has been recalibrated using spectral lines observed during long “day Earth” and “night Earth” observations. This allowed for more precise measurement of the azimuthal variation of gain across the detector, which is typically smaller than the radial gain variations.

The four gain corrections (short and long term gain variation, gain positional dependence and long term variation of the positional dependence), were carried out

at GSFC in the standard processing (Ebisawa, private communication). The Perseus observations analyzed in this work do have the standard gain corrections applied with the ftool **ASCALIN** v0.9t, which reads the gain correction coefficients at the time of observation from the gain history file. The gain correction coefficients were created by the ftool **TEMP2GAIN** v4.2, which reads the variation of the temperature housekeeping parameters, and registers the gain values for every 600 seconds of observation taking into account the long-term and positional gain variations (Idesawa et al. 1995).

Since there are still observed small redshift fluctuations measured with GIS 2 and, especially, GIS 3 for the same region, we assume that, in spite of the standard gain correction, there are still residual gain variations and we also assume, conservatively, that the magnitude of the residual gain fluctuations are on the same order as the fluctuations of the gain observed using the instrumental copper fluorescent line at 8.048 keV (Tashiro et al. 1999). Since the gain fluctuations increase with time, we use the 1997 data as our standard of reference. The radial gain distribution shows that if one excludes the very outer region ($r \geq 22'$) and the very central region ($\leq 2.5'$) from the spectral analysis the gain fluctuation around the mean is $\leq 0.15\%$, for both GIS 2 & 3. For all pointings observed in this work we extract spectra from a circular region with a $20'$ radius. The exclusion of the central $2.5'$ from the pointings with discrepant redshifts doesn't change our results. This is not surprising, since they are offset pointings (most photons come from a specific direction and not from the detector's center).

However, the direction from which most photons are detected for pointings P1 and P5 are different, so we also need to estimate the azimuthal gain variations. We also used the gain map determined using the Cu-K line at 8.048 keV (Idesawa et al. 1995). We compare the average gain values (excluding the outermost ring) of the region encompassing a 90° slice corresponding to the direction towards the real cluster's center (which is out of the field of view) for each instrument. This should give a good idea about the magnitude of the gain fluctuations as a function of detector's position for our observations. Although the gain differences for the GIS 2 obtained this way imply a small gain variation ($\sim 0.12\%$), for the GIS 3 the derived gain fluctuation is substantially larger ($\sim 0.37\%$) than that observed for the radial variations.

4.3. Redshift Dependence on Gain

In order to test the sensitivity of our observations to possible residual gain variations across the GISs we used Monte Carlo simulations. Supposing the redshift to be constant for the two discrepant regions, we generated fake spectra for both the GIS 2 & 3 for the

two pointings and compare the best-fit redshift differences. We can then calculate the probability that we find the same redshift differences (or greater than) that we observe in the real pointings for GIS 2 & 3. We simulated 1000 GIS 2 & 3 spectra corresponding to each real observation using XSPEC tool `fakeit`. In generating the fake spectra we used the same spectral model (`wabs mekal`) that we used for fitting the real data with the values of temperature, abundance, N_H and normalizations correspondent to the real best-fitting values of each pointing. We used the actual background spectra extracted within the same spatial extraction region for each pointing and effective exposures corresponding to the real pointing being simulated. We also used the responses (ARF and RMF) corresponding to the real pointings. Count statistics were incorporated in the generated spectra. For all simulations we set the redshift to that obtained through the spectral fittings of the central pointing ($z = 0.025$).

Each simulated spectrum was then grouped (25 cnt/channel) and fitted in the same way as the real ones and the best-fit values of the redshift were recorded. We then selected the simulated spectra that had a redshift difference equal to or greater than that observed in the real pointings for both GIS 2 & 3 (0.0208 for GIS2 and 0.0302 for GIS3). Gain effects do not enter directly in the procedure of generating simulated spectra. Therefore, in order to estimate the effects of GIS gain variations, we added a gain uncertainty to the best-fit values of redshift derived from fake spectra. We assume that the gain variations follow a Gaussian distribution with a standard deviation (σ_{gain}), which is different for each spectrometer, and a zero mean. This gain uncertainty is then summed to the best-fit redshifts obtained from the fake spectra before calculating the redshift differences between different pointings. To be conservative we assumed as our $1-\sigma$ gain variations (σ_{gain}) for the GIS 2 & 3 the largest values of the two procedures described above, i.e. 0.15% and 0.37% for GIS 2 & GIS 3, respectively.

The probability of observing the redshift differences in GIS 2 & 3 that we measure for the real spectra in two pointings (P1 and P5), using the procedure described above is found to be $\lesssim 0.005$. To illustrate how sensitive this value is to the assumed σ_{gain} we varied the estimated σ_{gain} and recalculated the probability of finding the redshift differences by chance. We plot the results in Figure 5 (for the purpose of illustration σ_{gain} for GIS 2 & 3 are assumed to be the same). It can be seen that this probability is rather insensitive to gain variations up to a σ_{gain} of $\sim 0.5\%$.

In a more realistic case we observe overall seven outer pointings and not only two. Therefore, we estimated the probability of finding the same redshift differences that we see in pointings P1 and P5 in seven observations using the same procedure to simulate spectra as described above. We also included a condition for alignment. Consider the line that

crosses a pointing P_j (which has a azimuthal angle PA_j) and the X-ray center of Perseus. Any pointing P_i (with azimuthal angle PA_i) will be considered to be aligned with pointing P_j if $(PA_j + \pi - A) \leq PA_i \leq (PA_j + \pi + A)$, where A is some alignment angle. Conservatively, we assume a broad alignment condition ($A = \frac{\pi}{3}$). The results are also shown in Figure 5 (thin line). Even in this case, the redshift difference is still significant at $\gtrsim 97\%$ confidence level.

5. Discussion

The spectral analysis of *ASCA* GIS 2 & 3 carried out in this work indicates the presence of a significant velocity gradient in the ICM of the Perseus cluster. Two regions show discrepant redshifts not just with respect to each other but also with respect to the central region. We have shown in the previous paragraphs that this difference is unlikely to be attributed purely to gain fluctuations and suggests the existence of large-scale bulk motions of the intracluster gas in this cluster. The temperature measurements show a general radial positive gradient, consistent with a cooling flow in the inner regions and an isothermal distribution in the outer regions. The abundance distributions are consistent with a global central abundance enhancement decreasing by about 30% outwards.

The two symmetrically opposed discrepant regions have velocity differences of ~ -3000 $km\ s^{-1}$ (or ≤ -600 $km\ s^{-1}$ at the 90% confidence level) for P_1 and $\sim +5000$ $km\ s^{-1}$ (or $\geq +60$ $km\ s^{-1}$ at the 90% confidence level) for P_5 with respect to P_0 . There are no observed temperature or abundance differences in the two pointings with discrepant redshifts (P_1 & P_5). The velocities measured are consistent with large scale gas rotation with a correspondent circular velocity of $\sim 4100 \pm^{2200}_{3100} km\ s^{-1}$ (90% confidence). This implies a large angular momentum for the ICM and that a significant fraction of the gas energy is kinetic⁴.

The best candidate for generating this large angular momentum is off-center mergers. In off-center mergers, up to $\sim 30\%$ of the total merger energy may be kinetic (can be transferred to rotation) (e.g. Pearce et al. 1994). Off-center merger simulations often produce residual intracluster gas rotation with velocities of a few $\times 10^3 km\ s^{-1}$ (e.g. Ricker 1998, Takizawa 1999, 2000, Roettiger & Flores 2000). Additional evidence for merging in Perseus comes from the observed: 1) offset between the optical center and the X-ray center (Branduardi-Raymont et al. 1981; Snyder et al. 1990; Ulmer et al. 1992), 2) radial change in X-ray isophotal orientation (isophotal twist)(Mohr, Fabricant, & Geller 1993) and 3)

⁴ Implying a correction on the measured specific energy of the gas, lowering β_{spec} and the $\frac{\beta_{spec}}{\beta_{imag}}$ discrepancy (Evrard 1990; Allen et al. 1992).

asymmetric galaxy morphological distribution, with preferential eastward direction in the distribution of E+S0 types (Brunzendorf & Meusinger 1999). However, simulations also indicate other observable consequences of mergers that can, in principle, be cross-analyzed with the velocity maps to test the robustness of the merger scenario. One of the features predicted by off-center cluster-cluster mergers is a strong negative radial temperature gradient (core heating) (≥ 2 keV/Mpc) for most of the merger life-time, even when the angle of view is not favored, e.g. along the collision axis (e.g. Takizawa 2000, Ricker 1998). In our case we do not observe a negative temperature gradient at all. Actually, we observe a positive temperature gradient due to the cooling flow. The mere fact that the cooling flow is present makes the off-center merger explanation more uncertain, since it has been suggested that a merger would disrupt any pre-existing cooling flows (e.g. Edge, Steward & Fabian 1992, Roettiger et al. 1993). However, recent simulations of head-on cluster mergers indicate that cooling flows can survive mergers depending on the produced ram-pressure of the gas in the infalling cluster (Gomez et al. 2000). Even if cooling flows are disrupted in a merger they can be reestablished quickly if the cooling time of the primary pre-merger component is small (Gomez et al. 2000). The fact that the major axis of the X-ray elongation is relatively close to the apparent rotation axis is another difficulty posed to the off-merger explanation. In most cases the isodensity contours are elongated perpendicularly to rotation axis, except in some short-lived merger stages viewed from specific directions (e.g. Takizawa 2000).

Two options to try to conciliate the velocity gradients that we find with merger scenarios are: 1) we are seeing a pre-merger stage with an infalling sub-group; 2) The merger happened long ago and the cluster was able to reestablish a cooling flow (and create a central metal abundance gradient) or the central region has not been disrupted. Against the former scenario is that we do not observe X-ray surface brightness enhancement at the direction of the redshift-discrepant regions. *ROSAT* PSPC images of P5 do not show any source bright enough to contaminate the overall flux and, consequently, the measured redshifts. However, we do observe a mild enhancement in surface brightness towards the East region of Perseus, coinciding with our P4 pointing. This enhancement was noticed previously by Schwarz et al. (1992) and Ettori et al. (1998) with better significance, and has been interpreted as evidence for merging group, which could also explain the lower temperatures detected towards the East by Schwarz et al. (1992). We do not detect a temperature gradient towards the East, but since our eastern pointing (P4) is in a region of higher N_H the lack of sensitivity of GIS to the hydrogen column density could mask a small temperature decline. However, in order to match the low temperatures found by

ROSAT in P4 N_H would have to be significantly higher⁵. Although there is no clear optical evidence of a sub-group towards the direction of P5 that corroborates this scenario, the region of surface brightness enhancement (P4) is associated with a high fraction of early-type galaxies (Brunzendorf & Meusinger 1999). Brunzendorf and Meusinger (1999) optically detected a possible cluster at $z \sim 0.05 \sim 90'$ north of NGC 1275. The position of this “cluster” coincides with a surface brightness enhanced region detected with *ROSAT* (Kowalski 1994)⁶. However, its location is far north (beyond the region analyzed by *ASCA* and closer to the region where we detect low redshifts, and it is unlikely to explain the redshift discrepancy that we find in P5 & P1.

The second scenario would imply that large rotational velocities can be maintained for longer periods of time (comparable to a Hubble time if cooling flows are disrupted in off-center mergers)⁷. In some off-center merger simulations high rotational velocities can be maintained for ≥ 3 crossing times (e.g. Ricker 1998). However, typically, the gas velocities are higher towards the central cluster’s regions, which could not be detected in Perseus. If cooling flows are not disrupted in off-center mergers, then the results are consistent with a large off-center merger event that took place roughly ≥ 4 Gyr (assuming a cluster mass of $5 \times 10^{14} M_\odot$ at a radius of 1 Mpc (Ettori et al. 1998) and that the rotating gas at ~ 7 keV is gravitationally bound).

Since we cannot measure the X-ray elongation along the line-of-sight to make better comparison with simulations and it is not clear whether cooling flows and central abundance gradients can actually survive mergers (e.g. McGlynn & Fabian 1984; Fabian & Daines 1991; Allen et al. 1992; Markevitch et al. 2000; Gomez et al. 2000), and, given the necessary poor spatial scale required to measure gas velocities reliably with the GISs, the results shown in this paper cannot constraint different merger scenarios accurately. However, it provides new challenges to numerical simulations of cluster mergers. Any merger explanation for the velocity differences observed in Perseus will have to take into account the presence of: 1) a moderately high cooling flow, 2)a central metal abundance gradient and 3) a chemical gradient, i.e., a central dominance of SN Ia ejecta (Dupke & Arnaud 2000). Velocity measurements of the intracluster gas with *Chandra* and, especially, *XMM-Newton* satellites will be able determine ICM velocities in the central regions more precisely, thus providing

⁵Even when N_H was fixed to be twice as high for P4 as its correspondent Galactic value, the best-fit temperature found in that region was still 4.23 ± 0.13 with $\chi^2_\nu \sim 1.46$

⁶There is also a region of enhanced surface brightness $\sim 100'$ to the northeast of NGC 1275, also out of the region covered by *ASCA* (Kowalski, Personal Communication)

⁷The cooling time in the center of Perseus is ~ 1 Gyr and it is ~ 10 Gyr at ~ 200 kpc, where a mass deposition rate of $\sim 500 M_\odot \text{yr}^{-1}$ is inferred (Ettori et al. 1998).

information on the gas velocity curve, which will strongly constraint cluster-cluster merger models, or suggest alternatives for generating the large angular momentum observed.

We would like to thank, J. Arabadjis, G. Bernstein, M. Sulkanen, M. Ulmer and M. Takizawa for helpful discussions, J. Irwin for reading the manuscript and helpful suggestions and especially P. Fischer for the many helpful discussions and suggestions. The authors would particularly like to thank Dr. K. Ebisawa for providing information about *ASCA* GIS gain calibrations that was crucial to this work. We acknowledge support from NASA Grant NAG 5-3247. This research made use of the HEASARC *ASCA* database and NED.

REFERENCES

Allen, S. W., Fabian, A. C., Johnstone, R. M., Nulsen, P. E. J., & Edge, A.C. 1992, MNRAS, 254, 51

Anders, E., & Grevesse N. 1989, *Geochimica et Cosmochimica Acta*, 53, 197

Arnaud, K. A., Mushotzky, R. F., Ezawa, H., Fukazawa, Y., Ohashi, T., Bautz, M. W., Crewe, G. B., Gendreau, K. C., Yamashita, K., Kamata, Y., & Akimoto, F. 1994, *ApJ*, 436, L67

Arnaud, K. A. 1996, in *Astronomical Data Analysis Software and Systems V*, ASP Conf. Series volume 101, eds. Jacoby, G., & Barnes, J., p.17

Bevington, P. R. 1969, *Data Reduction and Error Analysis for the Physical Sciences* (New York: McGraw-Hill), p.200

Bird, C. M. 1993, PhD thesis, Minnesota University, Minneapolis

Branduardi-Raymont, G., Fabricant, D., Feigelson, E., Gorenstein, P., Grindlay, J., Soltan, A., & Zamorani, G. 1981, *ApJ*, 248, 55

Brunzendorf, J., & Meusinger, H. 1999, *A&AS*, 139,141

Dickey, J. M., & Lockman, F. J. 1990, *ARA&A28*, 215

Dottani, T., Yamashita, A., Ezuka, H., Takahashi, K., Crew, G., Mukai, K., & the SIS team 1997, *ASCA News* 5, April. (see also heasarc.gsfc.nasa.gov/docs/asca/gis sis_effective_area.html)

Dupke, R. A., & Arnaud, K. A. 2000, *ApJ*, submitted.

Dupke, R. A., & White, R. E. III 2000, *ApJ*, 537, 123

Crone, M. M., Evrard, A. E., & Richstone, D. O. 1996, *ApJ*, 467, 489

Edge, A. C., Stewart, G. C., & Fabian, A. C. 1992, MNRAS, 258, 177

Ettori, S., Fabian, A. C., & White D.A. 1998, MNRAS, 300, 837

Evrard, A. E. 1990, ApJ, 363, 349;

Evrard, A. E., Metzler, C. A., & Navarro, J. F. 1996, ApJ, 469, 494;

Eyles, C. J., Watt, M. P., Bertram, D., Church, M. J., Ponman, T. J., Skinner, G. K., Willmore, A. P., 1991, ApJ, 376, 23

Fabian, A. C. & Daines, S. J. 1991, MNRAS, 252, 17

Fitchett, M.J. 1988, in "Minnesota lectures on clusters of galaxies and large-scale structure", ed. Dickey, J. (San Francisco: Astronomical Society of the Pacific) p.143

Fritz, G., Davidsen, A., Meekins, J. F., & Friedman, H. 1971, ApJ, 164, 81

Gomez, P. L., Loken, C., Roettiger, K., & Burns, J. O. 2000, ApJ, submitted

Hwang, U., Mushotzky, R. F., Burns, J. O., Fukazawa, Y., & White, R. A. 1999, ApJ, 516, 604

Idesawa, E., Asai, K., Ishisaki, Y., Kubo, H., Kubota, A., Makishima, K., Tamura, T., Tashiro, M., & the GIS team 1995, heasarc.gsfc.nasa.gov/docs/asca/gain.html

Kaastra, J. S. 1992, An X-Ray Spectral Code for Optically Thin Plasmas, (Internal SRON-Leiden Report, updated version 2.0)

Katz, N., & White, S. D. M. 1993, ApJ, 412, 455;

Kowalski, M. P., Cruddace, R. G., Snyder, W. A., Fritz, G. G., Ulmer, M. P., & Fenimore, E. E. 1993, ApJ, 412, 489

Kowalski, M. P. 1994, in "The Soft X-ray Cosmos" ed. E. M. Schlegel & R. Petre., 363

Liedahl, D. A., Osterheld, A. L., & Goldstein, W. H. 1995, ApJ, 438, L115

McGlynn, T. A., & Fabian, A. C. 1984, MNRAS, 208, 709

Markevitch, M., Ponman, T. J., Nulsen, P. E. J., Bautz, M. W., Burke, D. J., David, L. P., Davis, D., Donnelly, R. H., Forman, W. R., Jones, C., Kaastra, J., Kellogg, E., Kim, D.-W., Kolodziejczak, J., Mazzotta, P., Pagliaro, A., Patel, S., VanSpeybroeck, L., Vikhlinin, A., Vrtilek, J., Wise, M., & Zhao P. 2000, ApJ, submitted (astro-ph/0001269)

Mewe, R., Gronenschild, E. H. B. M., & Van den Oord, G. H. J. 1985, A&AS, 62, 197

Mewe, R., Lemen, J. R., & Van den Oord, G. H. J. 1986, A&AS, 65, 511

Mohr, J. J., Fabricant, D. G., & Geller, M. J. 1993, ApJ, 413, 492

Morrison, R., & McCammon, D. 1983, ApJ, 270, 119

Mushotzky, R. F., & Szymkowiak, A. E. 1988, in Cooling Flows in Clusters and Galaxies, ed. A. C. Fabian (Dordrecht: Kluwer), 53

Navarro, J. F., Frenk, C. S., & White, S. D. M. 1995 MNRAS, 275, 720

Pearce, F. R., Thomas, P. A., & Couchman, H. M. P. 1994, MNRAS, 268, 953;

Peres, C. B., Fabian, A. C., Edge, S. W., Johnstone, R. M., & White, D. A. 1998, MNRAS, 298, 416

Ponman, T. J., Bertram, D., Church, M. J., Eyles, C. J., Watt, M. P., Skinner, G. K., & Willmore, A. P. 1990, Nature, 347, 450

Ricker, P. M. 1998, ApJ, 496, 670

Roettiger, K., Burns, J. O., & Loken, C. 1993, ApJ, 407, 53;

Roettiger, K., Burns, J. O., & Loken, C. 1996, ApJ, 473, 651

Roettiger, K., Loken, C., & Burns, J. O. 1997, ApJS, 109, 307

Roettiger, K. & Flores, R. 2000, ApJ, 538, 92

Schindler, S., & Muller, E. 1993, A&A, 272, 137 ;

Schwarz, R. A., Edge, A. C., Voges, W., Boehringer, H., Ebeling, H., & Briel, U. G. 1992, A&A, 256, L11

Snyder, W. A., Kowalski, M. P., Cruddace, R. G., Fritz, G. G., Middleditch, J., Fenimore, E. E., Ulmer, M. P., & Majewski, S. R. 1990, ApJ, 365, 460

Takizawa, M., & Mineshige, S. 1998, ApJ, 499, 82;

Takizawa, M. 1999, ApJ, 520, 514

Takizawa, M. 2000, ApJ, in press (astro-ph/9910441)

Tashiro, M., Fukazawa, Y., Idesawa, R., Ishisaki, Y., Kubo, H., Makishima, K., Ueda, Y., & the GIS team 1995, ASCA News 3, August.

Tashiro, M., Kubota, A., Kubo, H., Ebisawa, K., & the GIS team 1999, heasarc.gsfc.nasa.gov/docs/asca/gisnews.html (see also — gain.html)

Ulmer, M. P., Cruddace, R. G., Fenimore, E. E., Fritz, G. G., & Snyder, W. A. 1987, ApJ, 319, 118

Ulmer, M. P., Wirth, G. D., & Kowalski, M. P. 1992, ApJ, 397, 430

Figure Captions

Fig. 1.— Distribution of the spatial regions for different pointings analyzed in this work. PSPC surface brightness contours of Perseus are overlayed on the central pointing (P0). The radius of each circular region is $20'$.

Fig. 2.— Azimuthal distribution of Temperature (TOP), Metal Abundance(MIDDLE), and Redshift (BOTTOM) as a function of the azimuthal angle (0 – 2π). First data point from the left for all plots corresponds to P1, increasing to P7 (last). In the temperature plot solid and dashed lines represent the 1σ confidence limits for the central pointing (P0) without and with an extra cooling flow spectral component, respectively. Circles represent best-fit temperatures when N_H is fixed at the Galactic value for each pointing. The dotted lines show the 1σ confidence limits for the central pointing (P0) without the cooling flow spectral component and N_H is fixed at the Galactic value. In both abundance and redshift plots solid lines show the the 1σ confidence limits for the central pointing. The dash-dotted lines show the best-fit abundance values for the central $4'$ obtained by Dupke & Arnaud 2000, for comparison. Errors for all plots are 1σ confidence.

Fig. 3.— Confidence contour plot for the redshifts measured for pointings P1 & P5. The three contours correspond to 68%, 90% and 99% confidence levels (outwards). The line of equal redshifts is also indicated. The contours are found for simultaneous spectral fittings of four data groups (P1 GIS 2&3 and P5 GIS 2&3), and the redshifts of both instruments are locked together for the same pointing.

Fig. 4.— Spectral fittings for the region around the FeK line complex for P1 and P5 in both GIS 2 (a) & 3 (b). The bottom plots show the residual to the best-fit model when the metal abundance is set to zero for GIS 2(a) & 3(b). Data points and best-fit models for P1 are represented by dark lines and for P5 by brighter lines.

Fig. 5.— Probability of finding redshift differences equal or greater than what we observe for the real data ($P1 \times P5$) by chance as a function of the standard deviation of the gain variation. The solid line represents this probability for two pointings. The dotted line represents this probability for two out of seven pointings with an alignment angle of 60° . An alignment angle of 90° would mean that 2 pointings would be aligned just by been on oposite relative hemispheres. σ_{gain} for GIS 2 & 3 are assumed to be equal in this plot for illustration purposes.

Table 1. Analyzed Pointings

Pointing	Sequence Number	Date Observed	RA (2000)	DEC (2000)	EXP ^a (ksec)	GIS CNT ^b (kcount)
P1(NW)	85002000	1997-02-15	03h17m42.07s	+41°56'54.6"	16.6	25
P2(N)	85001000	1997-02-14	03h19m34.25s	+42°07'33.2"	15.4	19
P3(NE)	85000000	1997-02-14	03h22m03.53s	+41°59'05.6"	19.7	23
P4(E)	83052000	1995-08-19	03h22m42.24s	+41°30'47.9"	17.5	33
P5(SE)	85003000	1997-02-16	03h21m47.21s	+41°02'44.9"	14.1	20
P6(S-SW)	85004000	1997-02-17	03h18m52.46s	+40°57'10.4"	23.4	33
P7(W)	85009000	1993-09-15	03h17m05.04s	+41°31'22.4"	17.4	33
P0(Center)	80007000	1993-08-06	03h20m08.57s	+41°36'24.1"	11.8	183

^aEffective Exposure (Average for GIS 2 & 3)

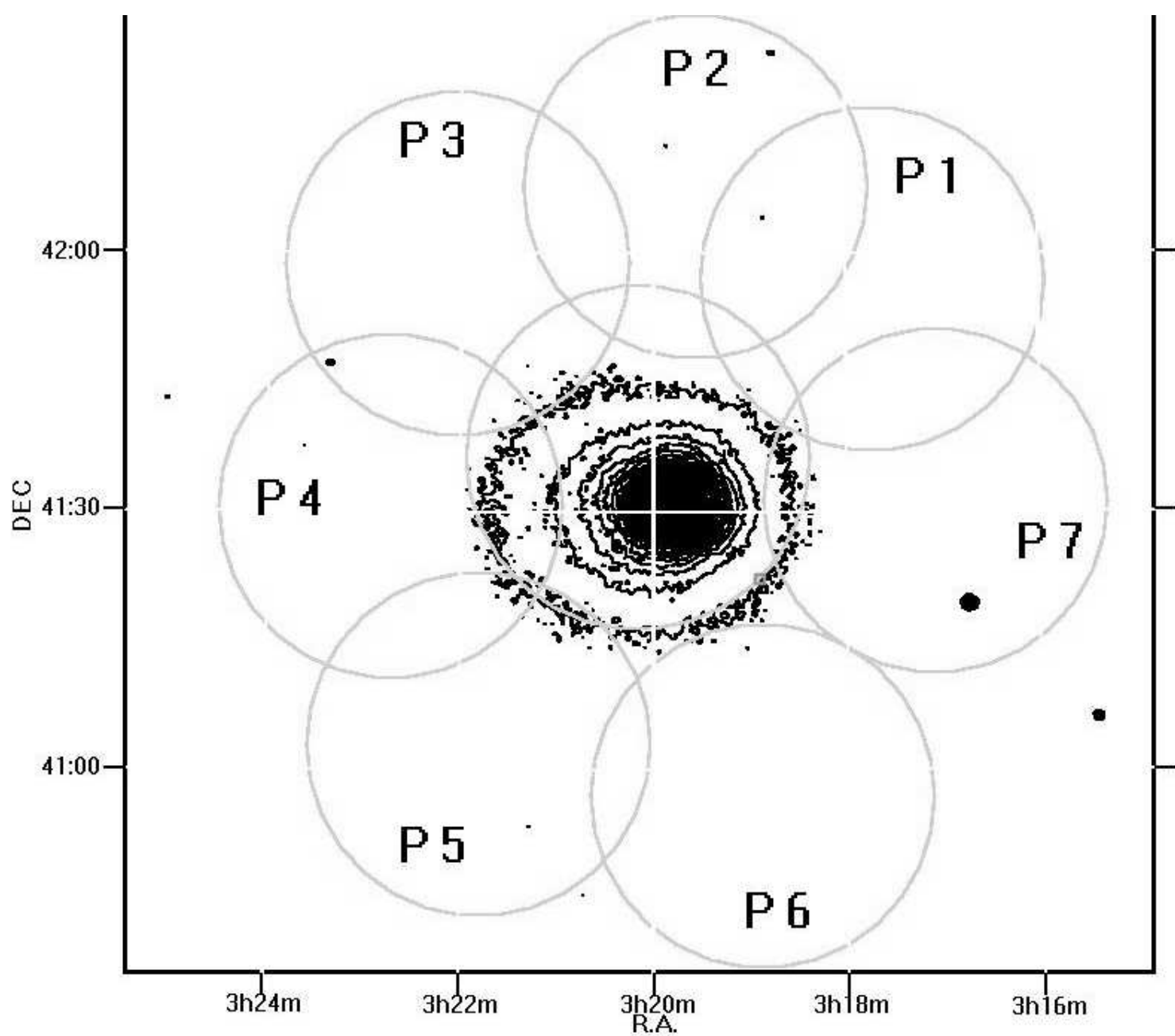
^bEffective Counts (Average for GIS 2 & 3)

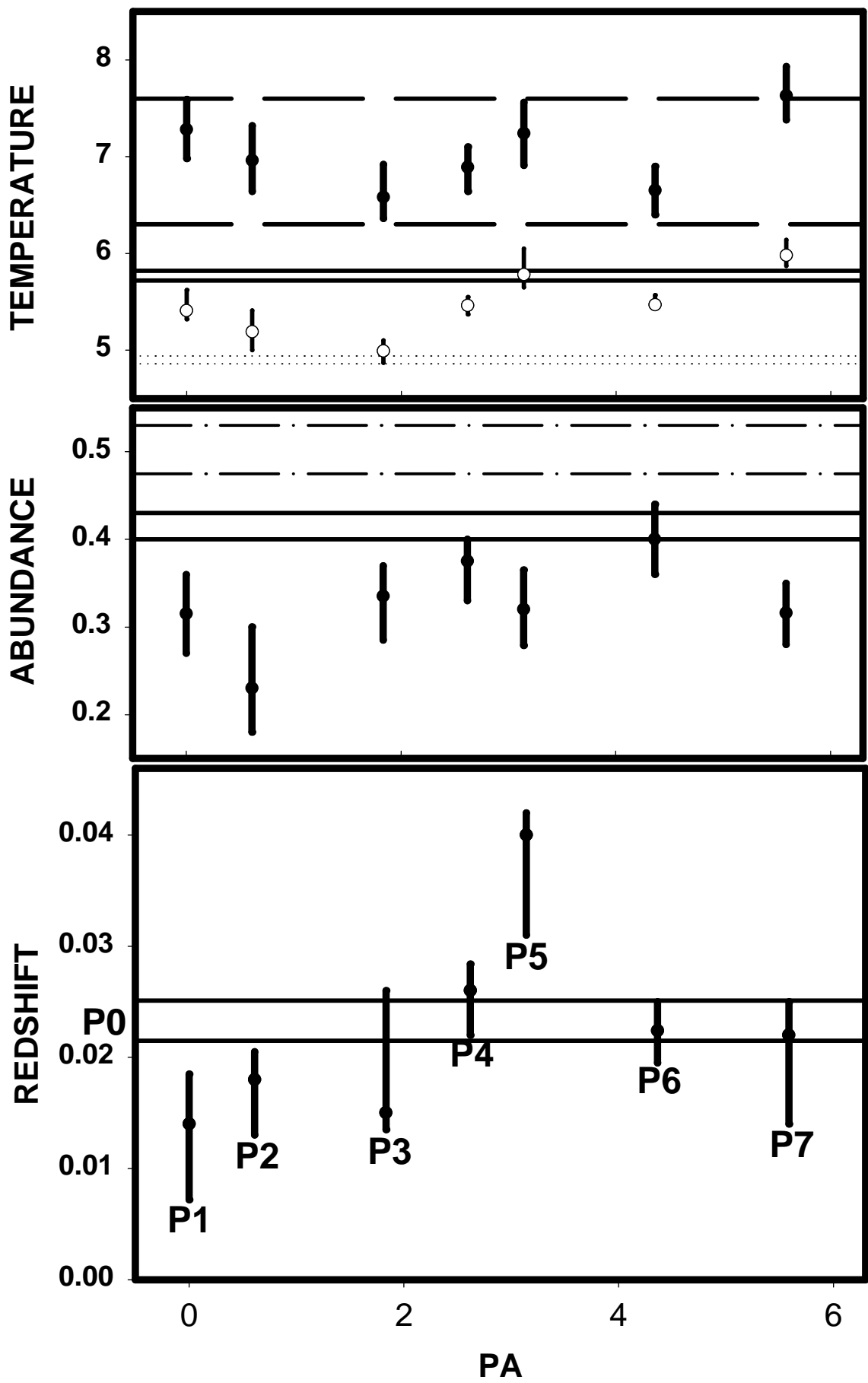
Table 2. Spectral Fittings^a

Pointing	Temp. (keV)	Temp. ^b (keV)	Abundance (Solar)	Redshift (10^{-2})	χ_{ν}^2
P1(NW)	$7.28_{-0.53}^{+0.44}$	$5.41_{-0.15}^{+0.22}$	$0.32_{-0.07}^{+0.07}$	$1.45_{-1.16}^{+0.40}$	1.054
P2(N)	$6.96_{-0.47}^{+0.48}$	$5.19_{-0.19}^{+0.21}$	$0.23_{-0.07}^{+0.08}$	$1.81_{-1.06}^{+1.20}$	1.097
P3(NE)	$6.58_{-0.48}^{+0.49}$	$4.99_{-0.19}^{+0.22}$	$0.34_{-0.08}^{+0.07}$	$1.6_{-0.87}^{+1.23}$	1.115
P4(E)	$6.89_{-0.35}^{+0.41}$	$5.46_{-0.15}^{+0.15}$	$0.38_{-0.06}^{+0.05}$	$2.64_{-0.76}^{+0.46}$	0.988
P5(SE)	$7.24_{-0.48}^{+0.56}$	$5.78_{-0.23}^{+0.27}$	$0.32_{-0.07}^{+0.07}$	$4.19_{-1.67}^{+0.33}$	1.006
P6(S-SW)	$6.65_{-0.33}^{+0.39}$	$5.47_{-0.12}^{+0.16}$	$0.40_{-0.06}^{+0.06}$	$2.19_{-0.62}^{+0.63}$	1.221
P7(W)	$7.63_{-0.41}^{+0.25}$	$5.98_{-0.18}^{+0.22}$	$0.32_{-0.06}^{+0.06}$	$2.16_{-1.36}^{+0.76}$	1.074
P0(Center)	$5.76_{-0.11}^{+0.11}$	$4.89_{-0.05}^{+0.05}$	$0.42_{-0.03}^{+0.02}$	$2.50_{-0.45}^{+0.00}$	1.067

^aErrors are 90% confidence level

^b N_H fixed at the corresponding Galactic value





Confidence contours

